

**This item is the archived peer-reviewed author-version of:**

Nanomechanical properties of SSTSAA microcrystals are dominated by the inter-sheet packing

**Reference:**

Meersman Filip, Quesada-Cabrera Raul, Filinchuk Yaroslav, Dmitriev Vladimir, Mcmillan Paul F.- Nanomechanical properties of SSTSAA microcrystals are dominated by the inter-sheet packing  
Philosophical transactions of the Royal Society : mathematical, physical and engineering sciences / Royal Society [London]- ISSN 1471-2962 - 381:2259(2023), 20220340  
Full text (Publisher's DOI): <https://doi.org/10.1098/RSTA.2022.0340>  
To cite this reference: <https://hdl.handle.net/10067/2003680151162165141>

# Nanomechanical properties of SSTSAA microcrystals are dominated by the inter-sheet packing

Filip Meersman<sup>1\*</sup>, Raúl Quesada-Cabrera<sup>2,3</sup>, Yaroslav Filinchuk<sup>4</sup>,  
Vladimir Dmitriev<sup>5</sup>, Paul F. McMillan<sup>2</sup>

<sup>1</sup> Department of Chemistry, University of Antwerp, Groenenborgerlaan 171, 2020 Antwerp, Belgium

<sup>2</sup> Department of Chemistry, Christopher Ingold Laboratory, University College London, 20 Gordon St., London WC1H 0AJ, UK

<sup>3</sup> Department of Chemistry, Institute of Environmental Studies and Natural Resources (iUNAT), Universidad de Las Palmas de Gran Canaria, Campus de Tafira 35017, Las Palmas, Spain

<sup>4</sup> Institute of Condensed Matter and Nanosciences, Université catholique de Louvain, Place L. Pasteur 1, 1348 Louvain-la-Neuve, Belgium

<sup>5</sup> Swiss-Norwegian Beamlines at ESRF, Boite Postale 220, F-38043 Grenoble, France

**Keywords:** bulk modulus, amyloid fibril, compressibility, packing

---

## Summary

Amyloid fibrils have been associated with human disease for many decades, but it has also become apparent that they play a functional, non-disease related role in e.g. bacteria and mammals. Moreover they have been shown to possess interesting mechanical properties that can be harnessed for future man-made applications. Here, the mechanical behaviour of SSTSAA microcrystals has been investigated. The SSTSAA peptide organisation in these microcrystals has been related to that in the corresponding amyloid fibrils. Using high pressure X-ray diffraction experiments the bulk modulus  $K$ , which is the reciprocal of the compressibility  $\beta$ , has been calculated to be 2.48 GPa. This indicates that the fibrils are tightly packed, although the packing of most native globular proteins is even better. It is shown that the value of the bulk modulus is mainly determined by the compression along the  $c$ -axis, that relates to the inter-sheet distance in the fibrils. These findings corroborate earlier data obtained by AFM and molecular dynamics simulations that showed that mechanical resistance varies according to the direction of the applied strain, which can be related to packing and hydrogen bond contributions. Pressure experiments provide complementary information to these techniques and help to acquire a full mechanical characterisation of biomolecular assemblies.

## Introduction

\*Author for correspondence (filip.meersman@uantwerpen.be).

Amyloid fibrils have been the focus of intensive investigation over the last few decades. This has been due to their elusive structure, their association with neurodegenerative and other amyloid-related diseases and the fact that the ability of their formation seems to represent a basic property of any polypeptide chain under the right conditions [1]. Although initially these macromolecular structures were thought to exist only in association with human disease, it has become clear that similar amyloid-like structures are found in, for instance, bacteria, algae, plants and even mammals [1-5]. These findings have given further credence to the notion of amyloid fibrils as a fundamental part of polypeptide chain behaviour. But along came the realisation that such structures should not necessarily be associated with human disease, but rather have emerged as natural functional macromolecular assemblies. Functional amyloids have been found to be involved in, for instance, natural adhesives, plant seed maturation, bacterial biofilm formation and hormone storage [2-5]. Moreover, it is now clear that we can exploit them technologically in a wide range of applications [6-8]. Not unlike the way collagen-derived polypeptides are used in bio-engineering to produce aerogels (to serve as haemostatic sponges, for example) or hydrogels [9, 10]. In this context, one particular feature of amyloid fibrils that has come to the fore is their high mechanical strength [11].

The mechanical behaviour has been widely investigated with a view on potential applications, but also as a way to gain further insight into the amyloid fibril structure and its formation [12-15]. Atomic force microscopy and molecular dynamics simulations are often the preferred tools to evaluate the mechanical properties [12, 14, 16-18]. We have previously studied the mechanical behaviour of TTR<sub>105-115</sub> amyloid fibrils and cellulose using high-pressure X-ray diffraction and Raman spectroscopy [19,20]. In the case of TTR<sub>105-115</sub> fibrils we were able not only to determine the bulk modulus of the fibrils but also to demonstrate the anhydrous nature of the inter-sheet space as was proposed based on peptide microcrystalline models [21,22]. The advantage of the high-pressure methodology is that it allows us to determine a bulk modulus as the sample is hydrostatically compressed, in contrast to the unidirectional strain or stretching applied in many other methods. However, the disadvantage of the TTR<sub>105-115</sub> fibrils as a model system was that we had to make assumptions on their unit cell in order to calculate the bulk modulus. Here we apply our approach to study the mechanical behaviour of SSTSAA microcrystals. These serve as a model for the amyloid fibril structure and their unit cell structure is well-defined [21]. SSTSAA is a hexapeptide derived from ribonuclease (RNase) and represents the minimum amino acid sequence of RNase that can form amyloid fibrils.

## Materials and methods

SSTSAA peptide was purchased from Eurogentec (Liège, Belgium). The peptide purity was assessed by HPLC and mass spectrometry (see Supporting Information). Microcrystals were prepared using the hanging-drop vapor diffusion method as described previously [21]. Briefly, a drop was a 1:1 mixture of a 30 mg/mL aqueous SSTSAA solution and a reservoir solution. The latter was composed of 0.1 M Na HEPES, pH 7.5, 10% v/v 2-propanol and 20% w/v polyethylene glycol 4000. Optical observations of the microcrystals were made using a Leica MZ125 light microscope with an ultra-long working distance lens (20x). Images were acquired with a digital camera (Fujifilm FinePix F40fd).

In situ high-pressure X-ray diffraction measurements on the microcrystals were performed using a diamond anvil cell, where the sample was contained within a 200- $\mu$ m hole drilled in a Re gasket. The pressure was determined using the ruby fluorescence method. X-ray diffraction data were collected at the Swiss-Norwegian beamline ( $\lambda=0.70026\text{\AA}$ ) at the European Synchrotron Radiation Facility (Grenoble, France) using a MAR345 image plate detector [23]. The sample-to-detector distance (300 mm) and the image plate inclination angles were calibrated using a LaB<sub>6</sub> standard. All experiments were performed at ambient temperature.

All obtained raw 2D images were transformed to powder diffraction patterns using the Fit2D program [24] and calibration measurements of a standard sample. This program was also used to remove diffraction spots

---

from the diamond cell and ruby used for pressure calibration. The crystal structure of SSTSAA reported in Sawaya et al. [21] was used in Rietveld refinements with the program Fullprof [25]. 9 parameters were varied: one scale, 3 cell and 3 profile parameters (pseudo-Voigt function), one variable accounting for a preferred orientation along [010] using March-Dollase model and an overall atomic displacement factor. The background was defined by a number of fixed points. Diffraction peaks were detectable up to the highest resolution shell, 1.64 Å. Cell parameters were extracted from data collected up to 1.4 GPa pressure. Beyond this limit the peaks broadened considerably.

The bulk modulus ( $K_0$ ) and its pressure derivative ( $K_0'$ ) were calculated using a finite-strain Birch-Murnaghan equation of state expanded to the third order using (Eq. 1) [26]:

(Eq. 1)

The volume strain  $f$  is given by Equation 2:

(Eq. 2)

Here  $V$  is the unit cell volume at a given pressure and  $V_0$  is the volume at ambient pressure.

## Results and discussion

Figure 1a shows a microscopy image of the SSTSAA microcrystals, analogous to the needle-like hay stacks observed by Sawaya et al. [21]. The microcrystals were used as such in the diamond anvil cell using their mother liquid as a pressure-transmitting medium. Because of the random orientations of the small individual needles the diffraction pattern (Fig. 1b) shows isotropic rings rather than single crystal-like diffraction spots. The microcrystals were gradually exposed to high hydrostatic pressures up to 12.8 GPa (1 GPa = 10 kbar). Compression beyond 8 GPa leads to the disordering of the crystalline structure but the process is reversible upon decompression. Here we focus on the pressure effects up to 1.4 GPa as the data in this pressure range can be well modelled by the Rietveld method. The atomic coordinates were fixed, refining the profile parameters, the unit cell and the overall atomic displacement factor, along with the texture (March-Dollase model) along the [010] direction. Figure 2 shows the unit cell at ambient pressure and at 1.4 GPa. The variation of the unit cell dimensions under compression is shown in Figure 3a. It can be seen that compression is anisotropic, with the long a-axis being the least compressible and the intermediate length c-axis the most compressible. It is very often the case that the compressibility is the highest in the direction normal to the molecule layers [27]. This also corroborates our earlier results on TTR<sub>105-115</sub> amyloid fibrils that showed that the inter-sheet distance, corresponding to the c-axis in the microcrystals, is more compressible than the inter-strand distance [19]. Nevertheless, the inter-sheet distance does not undergo a major compression, reflecting the densely packed interface or so-called dry steric zipper between the peptides. The b-axis can be related to

the distance between two strands along the apparent fibre axis. Its compressibility can mainly be ascribed to a shortening of the inter-strand hydrogen bonds which is found to be  $-0.074 \text{ \AA GPa}^{-1}$ . For comparison, the average hydrogen bond shortening in a native protein is  $-0.1 \text{ \AA GPa}^{-1}$ , and  $-0.09 \text{ \AA GPa}^{-1}$  in ice-Ih and  $-0.016 \text{ \AA GPa}^{-1}$  in a molecular crystal of pentaerythritol [28-31]. It is, however, noteworthy that these changes in the intermolecular distances do not necessarily have to be due solely to hydrogen bond shortening. Studies on molecular organic solids have shown that conformational changes and rotation of the molecules can also lead to optimised packing within the crystal. Though there is no evidence of such conformational change or rotation in this case, at least not in the pressure range up to 1.4 GPa.

The pressure dependence of the relative volume change  $V/V_0$  is shown in Figure 3b. Monitoring the unit cell's volume as a function of pressure allows the determination of the equation of state (EOS) of the microcrystals. Several EOS models exist [32]. Here we use the Birch-Murnaghan EOS, which is a modification of the Murnaghan EOS and which assumes a non-linear variation of the bulk modulus with pressure. A fit of the EOS to the data provides us with the bulk modulus  $K$  and its pressure derivative. The bulk modulus is one of the four elastic constants, the other being the Young's modulus, the shear modulus and Poisson's ratio [32]. The bulk modulus is the reciprocal of the isothermal compressibility  $\beta$  and thus provides a view on how the unit cell volume changes under compression. Note that the unit cell shape should not change, as that would imply a phase transition. The analysis yields a bulk modulus  $K$  of  $2.48 \pm 0.14 \text{ GPa}$  and a pressure-derivative  $K'$  equal to  $8.54 \pm 0.80 \text{ GPa}$ . This value is similar to that reported for TTR<sub>105-115</sub> fibrils [19] and is of the same order as the Young's moduli determined by AFM and computational methods [11, 12, 15, 17]. In fact, if we assume a Poisson's ratio of 0.3 [18] then we can calculate the Young's modulus of the SSTSA crystals to be 3 GPa. A  $K$ -value of 2.48 GPa corresponds to a compressibility  $\beta$  of  $0.4 \text{ GPa}^{-1}$ . It shows that the microcrystals and by extrapolation the amyloid fibrils are very well packed structures with little voids, making them relatively incompressible. Native proteins, however, often are even less compressible with typical values of  $\beta$  of  $0.1 - 0.2 \text{ GPa}^{-1}$  [32]. Although one should be careful when making comparisons as the structures of globular proteins and those of amyloid fibrils are so fundamentally different. It is also clear from Figure 3a that the value of the bulk modulus is largely determined by the compression in the direction normal to the apparent fibre axis in the microcrystals (i.e. the  $c$ -axis) (vide supra). This is in agreement with AFM and molecular dynamics simulations [14]. These have previously revealed that the mechanical response of amyloid fibrils depends on the direction of the applied strain. Packing is key in most directions, but along the fibril axis inter-strand hydrogen bonds provide additional resistance to stretch, as they also do under compression. It is noteworthy to point out that tensile experiments along the fibril axis tend to focus on the hydrogen bond breaking as a key element of their mechanical properties. Here the nature of the amino acid side chains, i.e. the amino acid sequence, is less important than the number and density of the hydrogen bonds [33]. Under compression, however, hydrogen bonds will in first instance be strengthened and the packing will be more important.

## Conclusions

Hydrostatic compression experiments on biomolecules and their assemblies such as amyloid fibrils and microcrystals provide unique access to a fundamental mechanical property being the bulk modulus and thus the compressibility. The extent to which a molecule or an assembly can be compressed gives insight into their packing. It has previously enabled us to provide experimental support for the dry steric zipper model in actual amyloid fibrils [19]. This methodology therefore offers information that complements AFM and molecular dynamics simulations, resulting a more complete picture of the mechanical behaviour of amyloid fibrils and model systems such as the microcrystals. In particular, simulations could provide a unique view on the role of hydration in the response of amyloid structures to the applied strain. It may also give insight into and allow the distinction between different fibril morphologies. Already at the level of the cross- $\beta$  structure

amyloid fibrils come in many shapes depending on the connectivity between the  $\beta$ -strands such as stacked or helical [33]. Their pressure response might reveal more about the underlying structure [33,34]. In this respect it is worthwhile to note that native proteins such as GFP, which has a  $\beta$ -barrel structure, and PemA, with its  $\beta$ -helix structure, have been found to be highly resistant to pressure-induced unfolding [35,36]. Apart from the fact that these proteins are well packed they also have a high areal hydrogen bond density, something that has been suggested to be important to achieve a stiff biological structure [33]. Albeit that these proteins are relatively short along their long axis compared to amyloid fibrils, they may nevertheless represent useful model systems to explore the mechanics of different morphologies, especially by simulations. The values of  $K$  and  $\beta$  reported here, suggest that the microcrystals are tightly packed, albeit not as tightly as native proteins. The mechanical properties under compression are dominated by the relative compressibility along the  $c$ -axis of the unit cell, corresponding to the inter-sheet distance in amyloid fibrils. SSTSAA has relatively small side chains. It would be interesting to see what the impact of larger side chains such as in the case of FYLLYY would be. Presumably here the packing in the dry zipper becomes less optimal and hence one would expect a higher compressibility. This might be exactly why there are different packing schemes, as shown by Sawaya et al. [21], or polymorphs of the cross- $\beta$  structure to avoid a structure that would be inherently less stable. From a materials point of view, this polymorphism and the associated different mechanical response may be exploited by selecting a specific morphology depending on the nature of the application and whether the system is supposed to withstand tensile or compressive strain.

## Acknowledgments

We thank Kristof Van Hecke (UGent, Belgium) for preparing the SSTSAA microcrystals and FNRS for the financial support. RQC would like to acknowledge the MEFP (Beatriz Galindo Program), Spain.

## References

1. Chiti, F., C. M. Dobson. 2006. *Annu. Rev. Biochem.* 75:333–366.
2. Mostaert, A.S., Higgins, M.J., Fukuma, T., Rindi, F., Jarvis, S.P. 2006. *J. Biol. Phys.* **32**, 393–401.
3. Antonets, K.S., Belousov, M.V., Sulatskaya, A.I., Belousova, M.E., Kosolapova, A.O., Sulatsky, M.I., Andreeva, E.A., Zykin, P.A., Malovichko, Y.V., Shtark, O.Y., Lykholay, A.N., Volkov, K.V., Kuznetsova, I.M., Turoverov, K.K., Kochetkova, E.Y., Bobylev, A.G., Usachev, K.S., Demidov, O.N., Tikhonovich, I.A., Nizhnikov, A.A. 2020. *PLoS Biol.* **18**, e3000564.
4. Akbey, Ü., Andreasen, M. 2022. *Chem. Sci.* **13**, 6457–6477.
5. Rubel, M.S., Fedotov, S.A., Grizel, A.V., Sopova, J.V., Malikova, O.A., Chernov, Y.O., Rubel, A.A. *Life* 2020, 10, 156; doi:10.3390/life10090156.
6. Lai, Y., Li, F., Zou, Z., Saeed, M., Xu, Z., Yu, H. 2021. *Appl. Mater. Today* **22**, 100966.
7. Biverstål, H., Kumar, R., Schellhaus, A.K., Sarr, M., Dantuma, N.P., Abelein, A., Johansson, J. 2020. *Sci. Rep.* **10**, 21765.

8. Diaz-Espinoza, R. 2022. *Nanomaterials* **12**, 3802.
9. Govindarajan, D., Duraipandy, N., Srivatsan, K.V., Lakra, R., Korapatti, P.S., Jayavel, R., Kiran, M.S. 2017. *ACS Appl. Mater. Interfaces* **9**, 16939–16950.
10. Xu, Q., Torres, J.E., Hakim, M., Babiak, P.M., Pal, P., Battistoni, C.M., Nguyen, M., Panitch, A., Solorio, L., Liu, J.C. 2021. *Mater. Sci. Eng. R* **146**, 100641.
11. Knowles, T.P., Fitzpatrick, A.W., Meehan, S., Mott, H.R., Vendruscolo, M., Dobson, C.M., Welland, M.E. 2007. *Science* **318**, 1900-1904.
12. Schleegeer, M., vanden Akker, C.C., Deckert-Gaudig, T., Deckert, V., Velikov, K.P., Koenderink, G., Bonn, M. 2013. *Polymer* **54**, 2473e2488
13. Grasso, G., Rebella, M., Morbiducci, U., Tuszynski, J.A., Danani, A., Deriu, M.A. 2019. *Front. Bioeng. Biotechnol.* **7**, 83
14. Ndlovu, H., Ashcroft, A.E., Radford, S.E., Harris, S.A. 2012. *Biophysical J.* **102**, 587–596.
15. Lamour, G., Nassar, R., Chan, P.H.W., Bozkurt, G., Li, J., Bui, J.M., Yip, C.K., Mayor, T., Li, H., Wu, H., Gsponer, J.A. 2017. *Biophysical J.* **112**, 584–594.
16. Volpatti, L.R., Knowles, T.P.J. 2014. *J. Polym. Sci. B: Polym. Phys.* **52**, 281–292.
17. Paparcone, R., Keten, S., Buehler, M.J., 2010. *J. Biomechanics* **43**, 1196-1201.
18. Guo, S., Akhremitchev, B.B. 2006. *Biomacromolecules* **7**, 1630-1636.
19. Meersman, F., Quesada Cabrera, R., McMillan, P.F. Dmitriev, V. 2011. *Biophys. J.* **100**, 193-197.
20. Quesada Cabrera, R., Meersman, F., McMillan, P.F., Dmitriev, V. 2011. *Biomacromolecules* **12**, 2178-2183.
21. Sawaya, M.R., Sambashivan, S., Nelson, R., Ivanova, M.I., Sievers, S.A., Apostol, M.I., Thompson, M.J., Balbirnie, M., Wiltzius, J.J.W., McFarlane, H.T., Madsen, A.Ø., Riek, C., Eisenberg, D. 2007. *Nature* **447**, 453-457.
22. Nelson, R., Sawaya, M.R., Balbirnie, M., Madsen, A.Ø., Riek, C., Grothe, R., Eisenberg, D. 2005. *Nature* **435**, 773-778.
23. Meersman, F., Quesada Cabrera, R., Filinchuk, Y., Dmitriev, V., McMillan, P.F., Primary XRD data. doi:10.5061/dryad.tdz08kq4b
24. Hammersley, A.P., Svensson, S.O., Hanfland, M., Fitch, A.N., Häusermann, D. 1996. *High Pressure Res.* **14**, 235-248.
25. Rodriguez-Carvajal, J. 1993. *Physica B* **192**, 55.
26. Jeanloz, R. 1998. *Phys Rev B* **38**, 805-807.
27. Boldyreva, E.V., 2008. *Acta Cryst. A* **64**, 218-23.
28. Williamson, M.P., Akasaka, K., Refaee, M. 2003. *Protein Sci.* **12**, 1971-1979.
29. Sivakumar, T.C., Chew, H.A.M., Johari, G.P. 1978. *Nature* **275**, 524-525.
30. Katrusiak, A. 1995. *Acta Cryst. B* **51**, 873-879.
31. Colloc'h, N., Girard, E., Dhaussy, A.C., Kahn, R., Ascione, I., Mezouar, M., Fourme, R. 2006. *Biochim. Biophys. Acta* **1764**, 391-397.
32. Ascione, I., Kahn, R., Girard, E., Prangé, T., Dhaussy, A.-C., Mezouar, M., Ponikwicki, N., Fourme, R. 2010. *J. Appl. Cryst.* **43**, 407–416.
33. Solar, M., Buehler, M.J. 2014. *Nanotechnol.* **25**, 105703.
34. Ostermeier, L., de Oliveira, G.A.P., Dzwolak, W., Silva, J.L., Winter, R. 2021. *Biophys. Chem.* **268**, 106506

- 
35. Scheyhing, C.H., Meersman, F., Ehrmann, M.A., Heremans, K., Vogel, R.F. 2002. *Biopolymers* **15**, 244-253.
36. Guillerm, J., Frère, J.M., Meersman, F., Matagne, A. 2021. *Biomolecules* **11**, 1083

## Figure and table captions

Figure 1: (a) Microscopy image and (b) diffraction pattern of the SSTSAA microcrystals.

Figure 2: (a) Rietveld refinement of diffraction patterns of SSTSAA at ambient pressure and 1.3 GPa. (b) Corresponding superposition of SSTSAA unit cells at 0.0001 GPa (blue) and 1.3 GPa (red), viewed along the c-axis. Here  $a_0 = 41,72\text{\AA}$ ,  $b_0 = 4,83\text{\AA}$  and  $c_0 = 12,72\text{\AA}$ . The crosses represent water molecules.

Figure 3: (a) Pressure-dependence of the normalised lattice parameters. (b) Variation of the unit cell volume with pressure. The data have been fit with Eq. 1 (solid line).

## Figures

Figure 1a



Figure 1b



Figure 2a

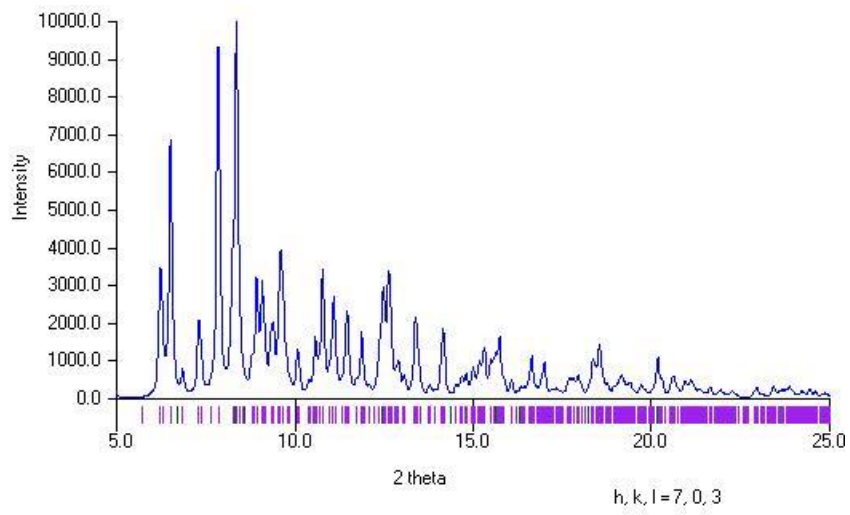


Figure 2b

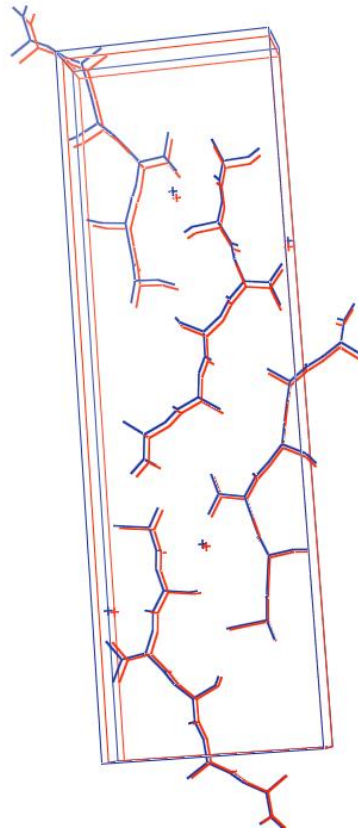


Figure 3a

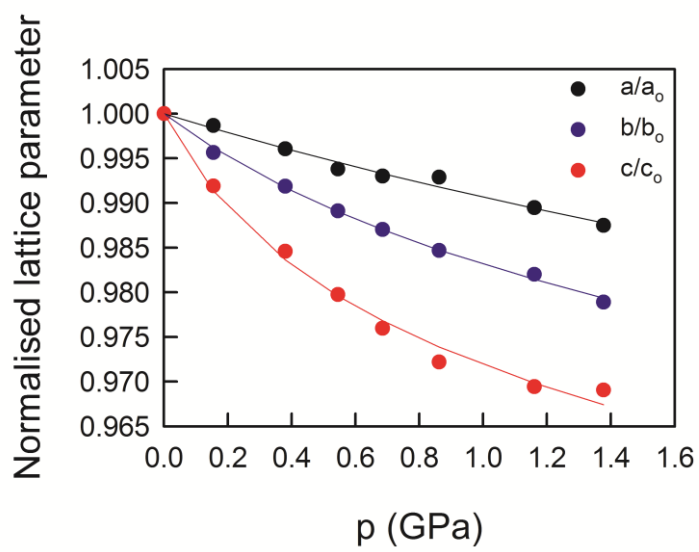
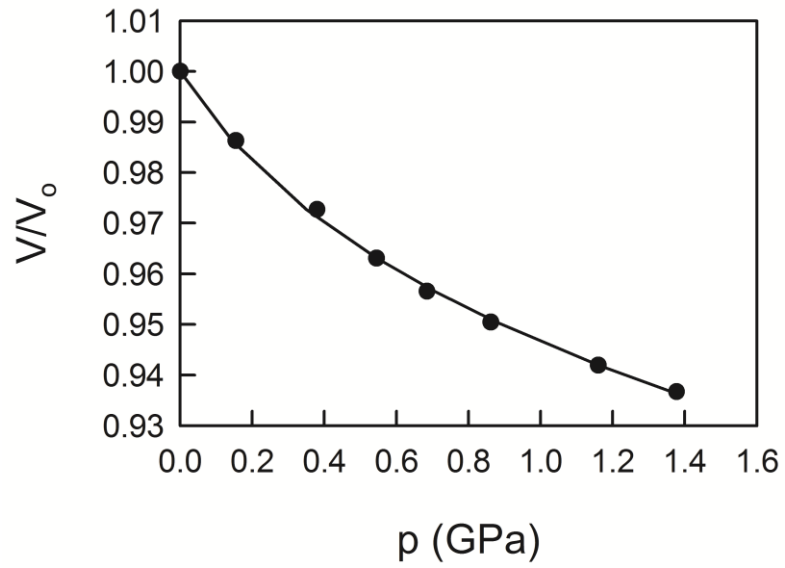


Figure 3b

**Competing Interests**

*We have no competing interests.*